*J Mater Sci: Mater Electron* (2020) 31:17044–17054

# Characterization of zinc lead-borate glasses doped with $Fe^{3+}$ ions: optical, dielectric, and ac-conductivity investigations

A. S. Abouhaswa[1,2,*], Y. S. Rammah[1], and Gamal M. Turky[3]

[1] Physics Department, Faculty of Science, Menoufia University, Shebin El-Koom, Menoufia 32511, Egypt
[2] Institute of Natural Science and Mathematics, Ural Federal University, Ekaterinburg, Russia 620002
[3] Department of Microwave Physics & Dielectrics, National Research Centre, 33 El-Bohouth St., Dokki, Giza 12622, Egypt

**Received:** 4 May 2020
**Accepted:** 14 August 2020
**Published online:** 28 August 2020



## ABSTRACT

The optical, dielectric response, and ac-conductivity properties for six glasses of zinc lead-borate doped with different contents of $Fe^{3+}$ ($Fe_2O_3$ = 0 to 10 wt%) have been investigated. UV–Vis spectra in 190–1100 nm wavelength have been carried out. Band gaps for optical energy ($E^{Optical}$), Urbach's energy ($E_U$), index of refraction ($n$), steepness parameter ($S$), energy dispersion parameter of refractive index ($E_d$), single-oscillator energy ($E_o$), the dispersion refractive index ($n_o$), minimum reflectance wavelength ($\lambda_o$), and oscillator strength ($S_o$) were evaluated. Results reveal that the indirect energy gap varies from 2.57 to 1.01 eV, while the direct energy gap takes values from 2.80 to 1.45 eV. The $E_U$ values change from 0.232 to 0.966 eV for glasses with $Fe_2O_3$ = 0 and 10 wt%, respectively. Also, $S$ and $\lambda_o$ decrease with the enhancement of $Fe_2O_3$ content. The dielectric response and ac-conductivity of the prepared glasses were investigated by broadband dielectric spectroscopy, BDS, in the frequency range from 0.1 Hz to 10 MHz and at temperatures ranging between 300 and 430 K. Two trends of activation plot have been observed in the conductivity of the samples with low content of $Fe_2O_3$. Although these samples show a perfect insulation features, they obey an anomalous behavior at higher temperatures. Therefore, the investigated glasses can be applied in several optical and opto-electronic devices.

## 1 Introduction

In the last decades, glass materials based on boron oxide ($B_2O_3$) have gained more attention from several researchers and investigators, due to their unique interesting physical and chemical characteristics such as good transparency, high transmittance, high chemical durability, low melting temperature, and high thermal stability. These properties lead the borate glasses to be applied in several applications as

Address correspondence to E-mail: aliabohaswa@hotmail.com


https://doi.org/10.1007/s10854-020-04262-1

luminescent materials, thermal and mechanical sensors, and as layers for both the opto-electronic and optical devices [1–5]. Introducing lead oxide (PbO) into borate glass systems helps to enhance the optical nonlinearity owing to high polarizability of $Pb^{2+}$ ions in glass networks [6]. On the other hand, association of PbO and $B_2O_3$ in the glass matrix plays double effect in the glass network: acts as glass former in the case of high boron oxide or acts as network modifier at low concentrations. Therefore, lead-borate glasses show large glass-forming range, which is useful for the manufacturing of structurally and optically different systems [7–9]. For the above reasons, lead-borate glasses were considered as good candidate materials in optoelectronic, photoelectric devices, and in optical switches. Broadband dielectric spectroscopy (BDS) became recently one of the main fruitful techniques for probing dynamic processes and the different mechanisms of the electrical conductivity in advanced glasses and glass ceramics owing to its extensive range of frequency and temperatures [10–14]. There are many studies focused recently on the effect of structure, temperature, and frequency on the electrical properties of conductive glasses [11, 14–20]. The electrical conductivity plays the main role of the variations in all dielectric values (such as permittivity, dielectric loss, electric modulus,…etc.) against frequency and temperature. In cases of ionic conductive glasses, the frequency dependence of the $\sigma'$ showed a plateau at the lower. The plateau represents the DC-conductivity ($\sigma_{DC}$) followed by a power law at higher frequencies. This behavior is now considered as a common feature in many other conducting polymeric systems and hydrogels [21–25]. AS the glass is of much higher conductivity, the electrical spectrum is characterized in the lower frequency (or at higher temperature) range by multistep decrease in the real part of conductivity, $\sigma'$. This phenomenon is due to the large bulk polarization taking place which is usually called as electrode polarization [15, 20, 26–29]. The electrochemical double layer builds up at the interface between the metallic electrode and the active material (electrolyte) originated from the existence of blocking electrodes which do not let the mobile ions to permit through external circuitry. In addition, there is also the interfacial polarization due to the heterogeneous structure of the considered conductive material. The correlation between both phenomena and the conductivity contribution on the dielectric spectra usually reflecting the higher rate of permittivity, $\varepsilon'$, increases which is very promising in the electrical energy storage technology.

In the present work, the optical, dielectric response, and ac-conductivity characteristics of zinc lead-borate glasses doped with $Fe^{3+}$ ions have been reported. To this end, the UV–Vis spectra for all investigated glasses were carried out in order to evaluate several optical properties. The conductivity of the proposed glasses was performed over wide frequency and temperature ranges. The electrical and dielectric responses of the studied glasses were investigated by broadband dielectric spectroscopy.

## 2 Materials and measurements

Six glass samples with chemical formula $50B_2O_3$-$10ZnO{\cdot}(40-x)PbO{\cdot}xFe_2O_3$, where ($x$ = 0, 1, 2.5, 5, 7.5 and 10), were prepared formerly by conventional melting method. The starting materials powders boron oxide ($B_2O_3$) (Sigma-Aldrich) 99.99%, zinc oxide (ZnO) (Winlab) 99.99, lead oxide ($Pb_3O_4$) (Alfa Aesar) 99.99%, and iron oxide ($Fe_2O_3$) (Sigma-Aldrich) 99.999 have been mixed very finely and preheated at 300 °C for 1 h. The resulting powders were then melted inside a porcelain crucible at temperature 1100 °C for 20 min and suddenly casted into a stainless steel mold to get the glass discs. After quenching the glass samples were immediately transferred for annealing in a muffle furnace adjusted at 300 °C. The preparation steps in detail are described in Ref. [30]. The optical measurements for the proposed glass samples were carried out utilizing JASCO UV–Vis–NIR spectrophotometer model V-570 in the wavelength ($\lambda$) range of 190–1100 nm (Table 1).

The electrical and dielectric quantities in the frequency range $10^{-1}$–$10^{7}$ Hz were achieved for all investigated glasses utilizing Novocontrol high-resolution alpha dielectric analyzer. This technique is supported by Quatro temperature controllers, using pure nitrogen as a heating agent and assuring temperature stability better than 0.2 K. The measurements were conducted using gold-plated brass electrodes of diameter 10 mm for upper electrode and 20 mm for the lower one in parallel plate capacitor configuration. All measurements were carried out at different temperatures ranging from RT (298) up to 473 K. The complex dielectrics function $\varepsilon^*(\omega,T)=\varepsilon'(\omega,T)-\varepsilon''(\omega,T)$, where $\varepsilon'$ is the

**Table 1** Codes and chemical composition in samples in the system $(50B_2O_3 - 10ZnO - (40 - x)\ PbO) + xFe_2O_3$: $0 \le x \le 10$ wt%) glasses [30]

| Sample code | Sample chemical composition |
|---|---|
| $x = 0$ | $50B_2O_3 - 10ZnO - 40\ PbO + 0\ Fe_2O_3$ wt% |
| $x = 1$ | $50B_2O_3 - 10ZnO - 39\ PbO + 1\ Fe_2O_3$ wt% |
| $x = 2.5$ | $50B_2O_3 - 10ZnO - 37.5\ PbO + 2.5\ Fe_2O_3$ wt% |
| $x = 5$ | $50B_2O_3 - 10ZnO - 35PbO + 5Fe_2O_3$ wt% |
| $x = 7.5$ | $50B_2O_3 - 10ZnO - 32.5\ PbO + 7.5\ Fe_2O_3$ wt% |
| $x = 10$ | $50B_2O_3 - 10ZnO - 30\ PbO + 10Fe_2O_3$ wt% |

permittivity and $\varepsilon''$ is the dielectric loss was obtained. It is equivalent with the complex conductivity function $\sigma^*(\omega, T) = \sigma'(\omega, T) + \sigma''(\omega, T)$ since, $\sigma^*(\omega, T) = i\omega\varepsilon_o\varepsilon^*(\omega, T)$, implying that $\sigma' = \varepsilon_o\omega\varepsilon''$ and $\sigma'' = \varepsilon_o\omega\varepsilon'$ ($\varepsilon_o$ being the vacuum permittivity).

## 3 Results and discussion

### 3.1 The optical characterizations

#### 3.1.1 UV–Vis spectroscopy

As mentioned before in Ref. [30], all investigated samples (x $Fe_2O_3$ = 0 to 10 wt%) were in glassy state and the color gradient of prepared glass samples is shown in Fig. 1. In order to evaluate the optical properties of the studied glasses, their UV–Vis spectra have been measured in the range of $\lambda$ = 190–1100 nm. Figure 2 depicts the normalized UV–Vis absorption spectra of $50B_2O_3$- + 10ZnO + (40 − $x$)PbO doped with $Fe_2O_3$ glasses at different values of $x$ = 0, 1, 2.5, 5, 7.5, and 10 wt%. From Fig. 2, spectra reveal that there are 3 robust and wide-ranging UV absorption band placed at about 240, 277, and 358 nm, tracked by a broad irregular near-visible band placed about 413 nm [31]. The broad near-visible band focused at about 413 nm shifted towards higher wavelength 655 nm with increasing $Fe_2O_3$ content. The extended visible absorption band at about 910 nm can be ascribed to the presence of ferric ions ($Fe^{3+}$) which added to the

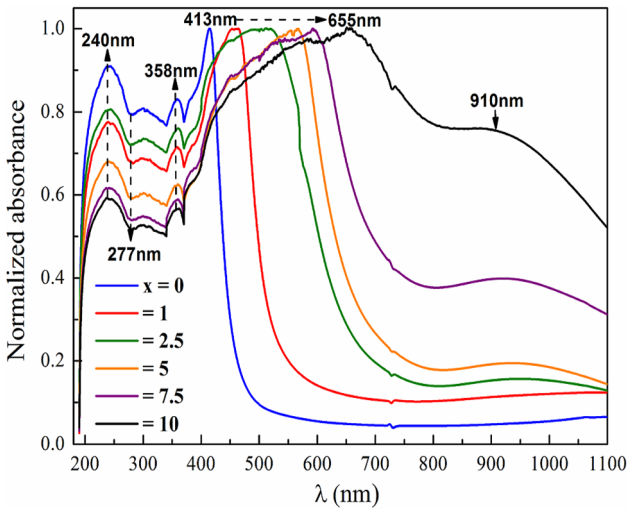


**Fig. 2** Normalized absorbance spectra of the investigated glasses.

samples and is ascribed to the transitions ${}^6A_{1g}(S) \rightarrow {}^4A_{1g}(G) + {}^4E_g(G)$ [32].

#### 3.1.2 $E^{Optical}$ and $E_U$

Direct and indirect band gaps of optical energy for the investigated glasses estimated utilizing their optical absorption coefficient $\alpha(v)$ with the help of absorbance ($A$) and thickness ($d$) of each sample was calculated utilizing the next relation [33]:

$$\alpha(v) = 2.303\left(\frac{A}{d}\right) = \left(\frac{1}{d}\right)\ln\left(\frac{I_o}{I}\right), \quad (1)$$

where $I_o$ and $I$ are the strengths of the incident and transmitted beams, respectively. Tauc's [34] and Mott and Davis [35] have been represented for Eq. (1) as

$$\alpha(v)hv = C(hv - E^{Optical})^m, \quad (2)$$

where $C$ is constant depends on the transition probability, the power $m$ points to the kind of electronic transition ($m$ = 1/2 for direct allowable transition and $m$ = 2 for indirect one) [35]. In Eq. (2), $E^{Optical}$ refers to the optical band gap energy of the sample. Variation of $(\alpha hv)^{1/2}$ and $(\alpha hv)^2$ with $hv$ for the investigated glasses is illustrated in Fig. 3a and b. With help of the spectra in Fig. 3a and b, the values of indirect ($E^{Optical}_{Indirect}$) and direct ($E^{Optical}_{Direct}$) optical energy band gaps can be

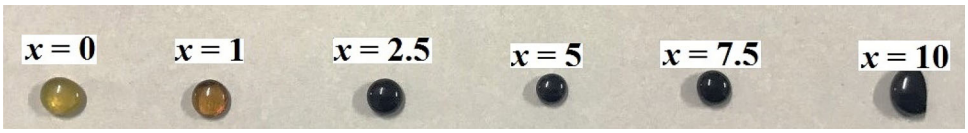


**Fig. 1** The color gradient of prepared glass samples.

evaluated via extrapolating the straight region of the graphs at the values at which $(\alpha hv)^{1/2}$ or $(\alpha hv)^2 = 0$. The results reveal that the indirect energy band gaps, $E_{\text{Indirect}}^{\text{Optical}}$ of samples decreased from 2.57 to 1.01 eV, while the direct energy band gaps, $E_{\text{Direct}}^{\text{Optical}}$ decreased from 2.80 to 1.46 eV as the $Fe_2O_3$ doping increased from $x = 0$ to 10 wt%. The reducing in direct and indirect band gap energies with increasing $Fe_2O_3$ content may be certified to the Fe faults within the bands, which mark the absorption of incident gamma-photons. The obtained $E_{\text{Indirect}}^{\text{Optical}}$ and $E_{\text{Direct}}^{\text{Optical}}$ values for all studied samples are collected and listed in Table 2.

In the present work, Urbach's energy ($E_U$) was used to describe the width of band tails as in the following relation [36]:

$$\ln(\alpha) = \ln(\alpha_0) + \frac{hv}{E_U}, \tag{3}$$

where $\alpha_0$ is constant and $E_U$ is the Urbach's energy. Drawing the variation of $\ln(\alpha)$ against $hv$ and estimating the inverse of slope for each plot, the corresponding value of $E_U$ can be obtained. Figure 4 shows the plots of $\ln(\alpha)$ against $hv$ and Table 2 includes the obtained values of $E_U$ for all the studied glasses. From Fig. 3 and Table 2, one can observe that the $E_U$ values increase as $Fe_2O_3$ content increases which connected to the creation of localized states in the band gap.

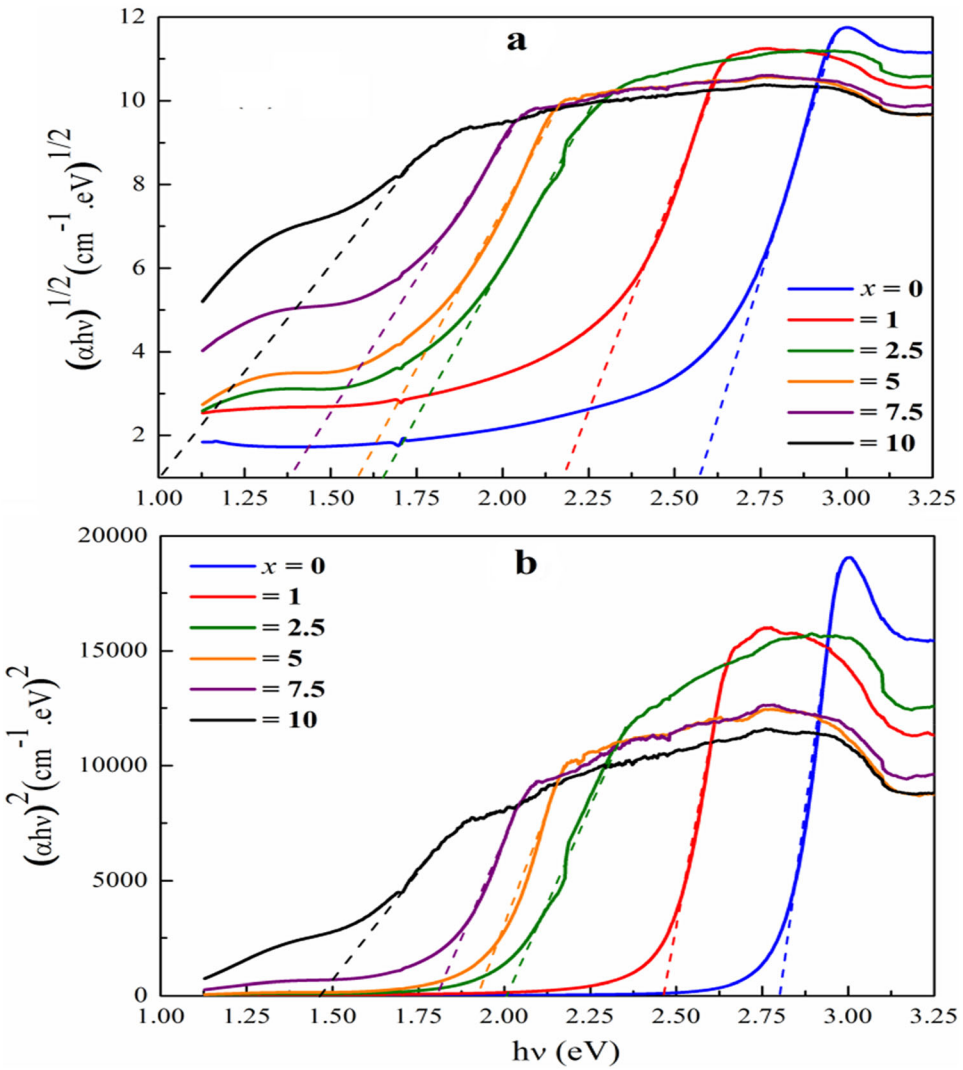


**Fig. 3** Variation of $(\alpha hv)^{1/2}$ and $(\alpha hv)^2$ with $hv$ for the investigated glasses.

**Table 2** $E^{Optical}$, $E_U$, $S$, $E_d$, $E_o$, $n_o$, $\lambda_o$, and $S_o$ for the investigated glasses

| Sample | $E^{Optical}$ (eV) | | $E_u$ (eV) | $S$ | $E_d$ (eV) | $E_o$ (eV) | $n_o$ | $\lambda_o$ | $S_o \times 10^{-4}$ |
|---|---|---|---|---|---|---|---|---|---|
| | Direct $E^{Optical}_{Direct}$ | Indirect $E^{Optical}_{Indirect}$ | | | | | | | |
| $x = 0$ | 2.80 | 2.57 | 0.232 | 0.111 | 2.812 | 3.675 | 2.99 | 75.96 | 13.76 |
| $x = 1$ | 2.46 | 2.17 | 0.264 | 0.098 | 2.884 | 3.354 | 3.03 | 71.35 | 16.06 |
| $x = 2.5$ | 2.00 | 1.65 | 0.382 | 0.068 | 3.052 | 2.851 | 3.74 | 66.69 | 29.20 |
| $x = 5$ | 1.92 | 1.57 | 0.521 | 0.050 | 3.984 | 2.142 | 4.38 | 62.35 | 46.77 |
| $x = 7.5$ | 1.80 | 1.36 | 0.731 | 0.035 | 6.604 | 1.532 | 4.79 | 55.35 | 71.62 |
| $x = 10$ | 1.45 | 1.01 | 0.966 | 0.026 | 10.249 | 1.025 | 5.05 | 50.23 | 97.11 |

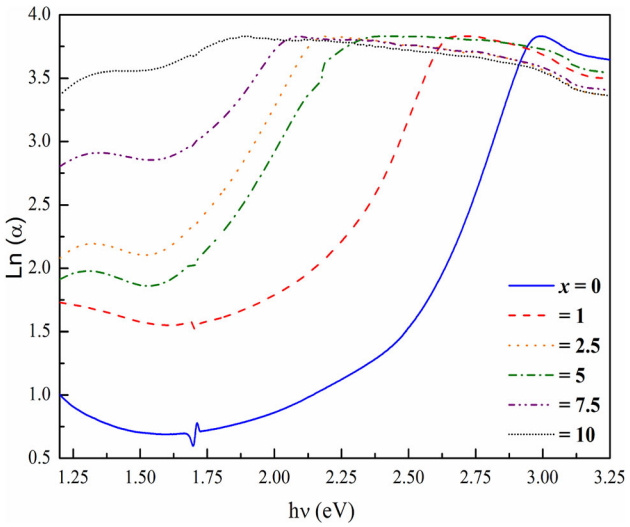


**Fig. 4** Ln(α) against $hv$ for the investigated glass samples.

### 3.1.3 Steepness parameter (S)

In addition, with help of $E_U$, the steepness parameter ($S$) which describes the mechanism of the exciton–phonon (electron–phonon) interactions by which the broadening of the absorption edge for the glass samples is created was calculated via [37]

$$S = \frac{k_\beta T}{E_U}, \tag{4}$$

where $T$ is the temperature in K° and $k_\beta$ is the Boltzmann constant. The obtained values of ($S$) are collected and listed in Table 2, the $S$ value decreases with the increae in $Fe_2O_3$ content approving the creation of localized states in the band gap [37].

### 3.1.4 T(λ), R(λ), and (n)

Dependence of transmittance $T(\lambda)$ and reflectance $R(\lambda)$ measurements for $50B_2O_3{\cdot}10ZnO{\cdot}(40 - x)PbO$ glass samples with different concentrations of $Fe_2O_3$ on $\lambda$ is plotted in Fig. 4. Plots in Fig. 5 show that the $T(\lambda)$ increases in the ultra-violet region but decreases in the visible region for all studied glasses, while plots of $R(\lambda)$ have an inverse behavior.

The index of refraction ($n$) for all glasses was evaluated according to [38]

$$n = \left(\frac{1+R}{1-R}\right) + \left(\frac{4R}{(1-R)^2} - k^2\right)^{1/2}. \tag{5}$$

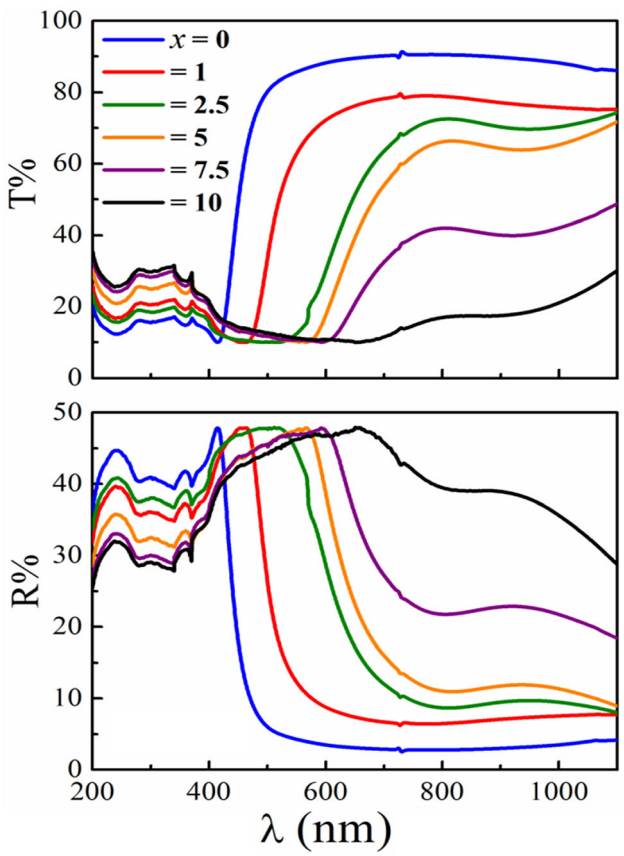


**Fig. 5** Dependence of $T\%$ and $R\%$ on $\lambda$ for all investigated glasses.

Here $R$ and $k$ represent the reflectance and the absorption index data, where $k = \alpha\lambda/4\pi$ [38]. The variation of ($n$) with ($\lambda$) for the proposed glasses is depicted in Fig. 5. From Fig. 6, it is seen that the ($n$) for samples enhances with the increasing $Fe_2O_3$ content. The values of ($n$) are considered as high, therefore, the studied glasses can be applied to develop the performance of photovoltaic and optical devices.

### 3.1.5 ($E_d$), ($E_o$), ($n_o$), ($\lambda_o$), and ($S_o$)

Additionally, parameter of the energy dispersion of refractive index ($E_d$) which evaluates the intensity of the interband optical transition for each glass sample can be evaluated utilizing the average of the single-oscillator energy ($E_o$) through the following relation [39].

$$(n^2-1)^{-1} = \frac{E_o}{E_d} - \frac{1}{E_o E_d}(h\nu)^2 \quad (6)$$

Via plotting $(n^2-1)^{-1}$ versus $(h\nu)^2$ for each glass sample as shown in Fig. 7, straight lines of each graph intercepts $y$-axis at a point = ($E_o/E_d$) and its slope = ($-1/E_oE_d$), then $E_d$ and $E_o$ can be evaluated. The $E_d$ and $E_o$ are presented in Table 2. The values of ($E_o$) reduce with increasing $Fe_2O_3$ content in the glass, i.e., it has the same trend of the optical energy gap, however, the ($E_d$) has an opposite trend.

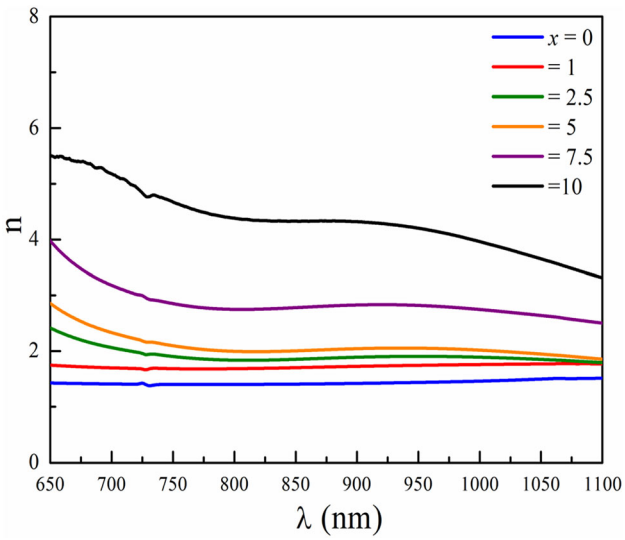


**Fig. 6** Dependence of refractive index ($n$) on $\lambda$ of the proposed glass samples.

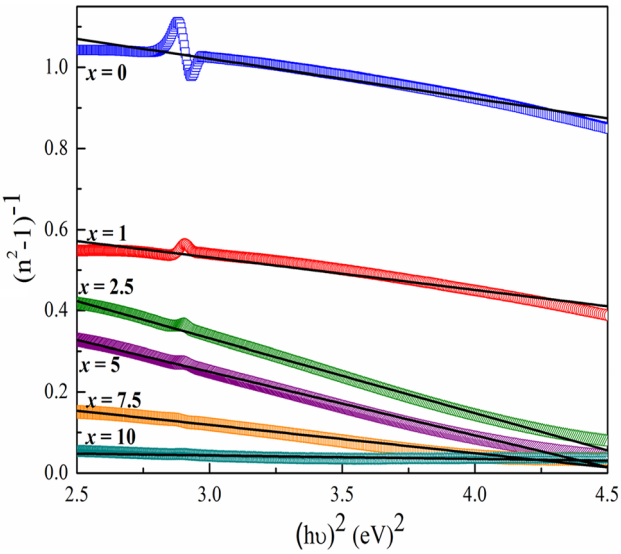


**Fig. 7** Variation of $(n^2-1)^{-1}$ with $(h\nu)^2$ of the proposed glass samples.

The dispersion refractive index ($n_o$) at zero energy photon (static refractive index) is calculated with help of the values of $E_o$ and $E_d$ as in Eq. (7) [39] and are listed in Table 2:

$$n_o^2 = \left(1 + \frac{E_d}{E_o}\right) \quad (7)$$

The values of $n_o$ for the studied glasses increase with increasing $Fe_2O_3$ concentration.

Finally, the wavelength values at a minimum reflectance ($\lambda_o$) for the studied glasses were evaluated utilizing Eq. (8) by drawing $(n^2-1)^{-1}$ versus $\lambda^{-2}$ as in Fig. 8 according to Moss model [40]:

$$\left(\frac{n_o^2-1}{n^2-1}\right) = 1 - \left(\frac{\lambda_o}{\lambda}\right)^2 \quad (8)$$

The average oscillator strength ($S_o$) can be evaluated with help of ($\lambda_o$) for all samples via Eq. (9) [39, 41]

$$S_o = \frac{(n_o^2-1)^2}{\lambda_o^2} \quad (9)$$

The obtained values of ($\lambda_o$) and ($S_o$) for each glass sample are listed in Table 2. It is clear that the ($\lambda_o$) decreases while the ($S_o$) increases with increasing $Fe_2O_3$ content.

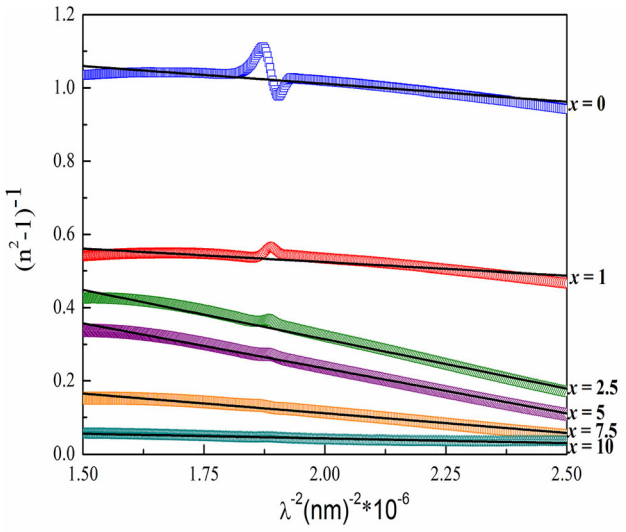


**Fig. 8** Variation of $(n^2 - 1)^{-1}$ with $(\lambda)^{-2}$ of the proposed glass samples.

## 3.2 Dielectric and electrical and investigations

The real part of the complex permittivity, $\varepsilon'$, for the studied glasses at ambient room temperature is depicted against frequency in Fig. 9. No remarkable effect of the frequency on the permittivity is noticed here reflecting the stability nature of the considered glasses. Also, the permittivity shows a very slight increase from 20 to 24 with increasing the concentration of $Fe_2O_3$ up to 10 wt % as shown on the inset of the figure. This gives the indication that the investigated glasses are dielectrically stable at room temperature against frequency of the external applied electric field and the doping with $Fe_2O_3$.

Also, the inset of the figure represents the effect of the $Fe_2O_3$ doping on the permittivity as determined at RT and frequency 1 kHz. In all cases a very low change of the permittivity could be seen here. This confirms, once again, the dielectric stability of the investigated glasses at ambient temperature. The measured permittivity, $\varepsilon'$, and ac-conductivity, $\sigma'$, are illustrated graphically, as a function of measuring temperature at spot frequency point 1 kHz, in Fig. 10 for the two glass samples ($x$ = 1 and 5) as a representative example. In this context, we will consider the real part of electric conductivity, $\sigma'$, as the ac-conductivity, $\sigma_{ac}$. Figure 10 shows linear increase of $\varepsilon'$

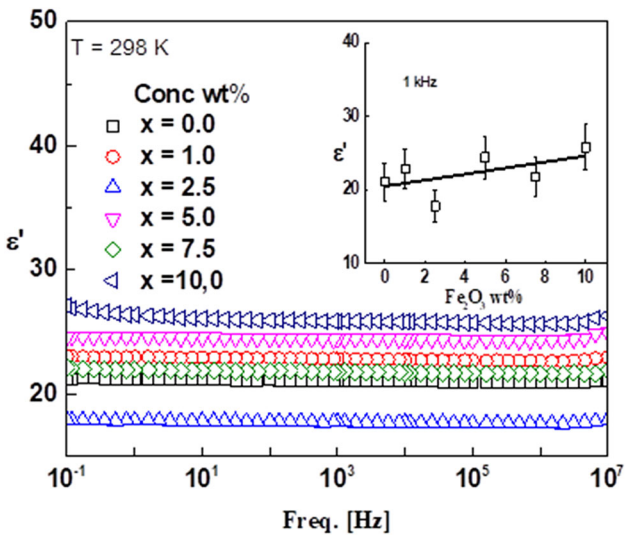


**Fig. 9** The permittivity, $\varepsilon'$ presented against frequency at RT for all samples under investigations. The inset shows the effect of concentration on the permittivity.

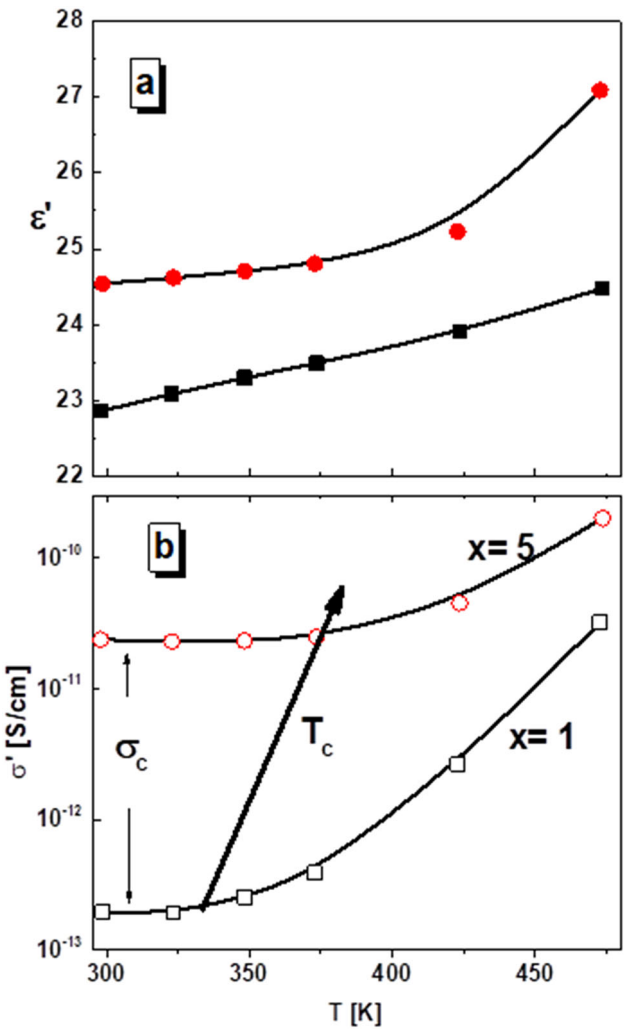


**Fig. 10** The permittivity, $\varepsilon'$ (**a**) and ac-conductivity, $\sigma'$ (**b**) as presented against temperature at 1 kHz for $x$ = 1 and 5 glasses.

with increasing temperature for the sample ($x$ = 1). This is due to the increase of the mobility of the charge carriers with heating, however, the rate of change is remarkably increasing and deviated from linearity in the case of the sample ($x$ = 5) at relatively higher temperatures. The abrupt increase of permittivity and hence of the ac-conductivity is attributed to the ferric ions ($Fe^{3+}$) which are added to the samples as temperature rose. Even though it is clear that the two glasses show a very good dielectric stability against heating since the increase of temperature from 300 to 475 is responded by increase of permittivity from 23 to 24 for the sample $x$ = 1 and from 24.5 to 27 for $x$ = 5, this may reflect the insulation features of the glasses under considerations. The real part of the complex conductivity $\sigma'$ is characterized on the low temperature side by a plateau-like behavior. The conductivity at that lower temperature range is constant ($\sigma_c$) and characterizes the structure of the investigated glass samples.

The characteristic temperature $T_c$, at which dispersion sets in and turns into a power law at higher temperatures, seems to be increased as $\sigma_c$. This behavior is somewhat like the behavior of the frequency dependence of $\sigma'$ for many conductive systems [42–45]. One has to notice that, $\sigma_{ac}$, in all cases and at all considered measuring temperatures as low as pico S/cm to nano S/cm which is in the range of insulating materials.

Figure 11 illustrates graphically the frequency dependence of permittivity, $\varepsilon'$, for the highly $Fe_2O_3$-doped glass ($x$ = 10) at different temperatures ranging from 25 to 200 °C. The figure shows that the value of permittivity attains a constant minimum value at

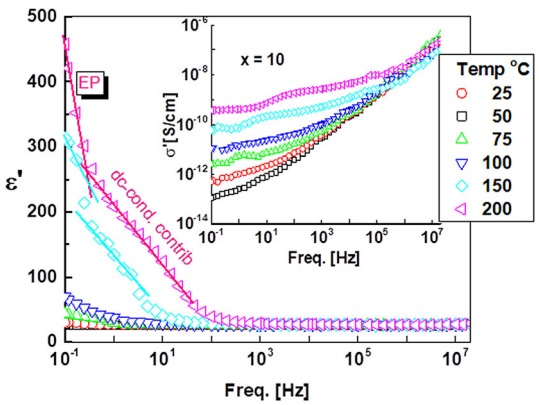


**Fig. 11** The real part of permittivity, $\varepsilon'$, as presented against frequency at various temperatures as indicated for the sample ($x$ = 10). Inset shows the debate plot of ac-conductivity.

higher frequencies collapsed for all considered temperatures. This could be explained by the lag of the polarizations' alteration behind that of the applied electric field. The values of, $\varepsilon'$, split up by decreasing the frequency according to the measuring temperatures. The other prepared glass compositions of high doping of $Fe_2O_3$ show analogous behavior. Two mechanisms are behind the abrupt increase at lower frequencies in values of permittivity, $\varepsilon'$ could be characterized by the two trends observed here. The first one originated from the accumulation of charge carriers at the interfaces: (a) between the electrodes and the material, due to the presence of blocking electrodes which do not allow the mobile ions to pass through external circuitry, this is called electrode polarization; (b) at the interfaces between different materials in heterogeneous structure and is produced by the separation of mobile positively and negatively charged particles under an applied field, which form positive and negative space charges in the bulk of the material. It is usually called space charge or Maxwell–Wagner–Siller, MWS, polarization. The correlation between them causes the abrupt increase of permittivity as the frequency decreases making the investigated glass promising for energy storage technology. The second trend is of lower rate of change and is accompanied by the hopping mechanism of charge carriers' transportations and correlated to the dc-conductivity. The latter is characterized by plateau-like behavior on $\sigma'$ representation as shown in the inset of the figure.

In order to report the influence of frequency, temperature, and composition on the ac- and dc-conductivity, the frequency dependence of $\sigma'$ of three different samples is depicted at two different temperatures in Fig. 12. Figure 12 shows linear decrease of $\sigma'$ with decreasing frequency at RT (298 K) for the sample of lower $Fe_2O_3$ ratio content (1 wt%) that is coincident with that of the $Fe_2O_3$-free sample. This behavior is the common feature of the perfect insulator glasses and it has a value of $\sigma'$ in the order of [4 × $10^{-15}$ S/cm (femto Siemens per cm)] at 0.1 Hz. As the ratio of $Fe_2O_3$ increases to 10 wt%, this value tends to be $10^{-13}$, i.e., 1.5 order of magnitude higher. However, the increase of measuring temperature up to 475 K enhances the dc-conductivity to about 3.5 decades higher for all investigated samples. By conducting more inspection of the figure at relatively higher temperature, two frequency-independent plateau regions were noticed. The plateau region at

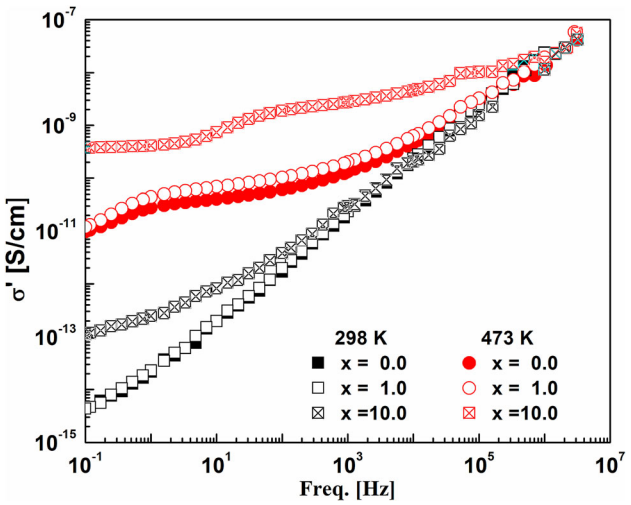


**Fig. 12** The real part of conductivity, $\sigma'$, as presented against frequency at two selected temperatures and for three selected samples as indicated.

low frequencies corresponds to the accumulation of charge carriers at the surface of the electrode–electrode polarization. It shifts remarkably towards lower frequencies as the temperature and/or the ratio of $Fe_2O_3$ decreases to be out of the considered window of frequency. The other plateau at intermediate frequencies correlates to the long-range defect migration of impurities that exhibits the dc-conductivity. The bend-like behavior shown at high frequencies highly corresponds to the structural relaxation process (α-process) that correlate with the interfacial polarization.

Figure 13 illustrated the temperature dependence of $\sigma'$@1 Hz which could be considered as the dc-conductivity $\sigma_{dc}$ at least for the semi- and highly conductive glasses. Figure 13 confirmed, once again, the insulation feature at relatively lower temperatures for the samples of $Fe_2O_3$ up to 0–5 wt%. There are two trends according to the range of temperature under consideration. The conductivity increases with low rate up to 70° C and then the rate tends to be much higher. The sample $x = 5$ has the lowest values of conductivity that attributed previously to the blocking effect of $Fe_2O_3$ on flow of charge carriers [46]. The activation plot of the two trends for the samples $x = 0$–5 and of the two samples of higher $Fe_2O_3$ ratios (7.5 and 10 wt %) follows an Arrhenius relation which reads [47, 48]

$$\sigma_{dc} = \sigma_{\infty} \exp\left(-\frac{E_A}{K_B T}\right), \quad (10)$$

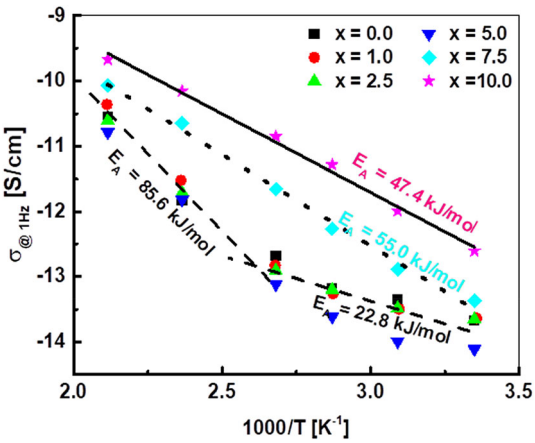


**Fig. 13** Arrhenius plot of the real part of conductivity, $\sigma'$, at one spot frequency point 1 Hz for $xFe_2O_3$ ($x$ = 0, 1, 2.5, 5, 7.5, and 10 mol%) glasses.

where $E_A$ is the activation energy, $K_B$ is the Boltzmann's constant, and $\sigma_{\infty}$ the dc-conductivity in the high-temperature limit. The calculated values of activation energy for all the samples are also shown in the plot for different glass compositions, which is calculated using Arrhenius temperature dependence. It can be observed that $\sigma_{dc}$ is increasing, and $E_A$ is decreasing for the sample of 10 wt% $Fe_2O_3$ in comparison with that of 7.5 wt %. This can be explained on the basis of the fact that the ferric ions ($Fe^{3+}$) which added to the samples have higher mobility which may result in the increase in conductivity and decrease in activation energy with increase in $Fe_2O_3$ content. The abrupt increase of the conductivity at relatively higher temperatures range for the glasses $x = 0$–5 wt% can be attributed to the increase of the ions' mobility. However, the accompanied increase of the activation energy does not agree with that view since the increase of $E_A$ should be due to something hindered the mobility which in turn decreases the conductivity which is not the case. Further work should be done in order to modulate and clarify that anomalous behavior.

## 4 Conclusion

The optical, electrical, and dielectric properties for six glasses of zinc lead-borate doped with different contents of $Fe^{3+}$ with chemical formula $50B_2O_3$ + 10ZnO + (40 − $x$) PbO + $xFe_2O_3$: $x$ = 0, 1, 2.5, 5, 7.5, and 10 wt% have been investigated. UV–Vis

spectra in 190–1100 nm wavelength have been carried out. Results reveal that the indirect energy gap varies from 2.57 to 1.01 eV, while the direct energy gap takes values from 2.80 to 1.45 eV of the proposed glasses. Urbach's energy ($E_U$) values change from 0.232 to 0.966 eV for glasses with $Fe_2O_3$ = 0 and 10 wt%, respectively. The wavelength values at a minimum reflectance ($\lambda_o$) decrease with enhancement of $Fe_2O_3$ content. The average of the single-oscillator energy ($E_o$) decreases from 3.675 to 1.025 for glasses with 0 to 10 wt% of $Fe_2O_3$ content. The energy dispersion parameter of refractive index ($E_d$) increases from 2.812 to 10.249 for glasses with 0 to 10 wt% of $Fe_2O_3$ content. The investigated glasses are dielectrically stable at room temperature against frequency of the external applied electric field and doping with $Fe_2O_3$. The ($\sigma_{ac}$) in all cases and at all considered measuring temperatures as low as pico S/cm to nano S/cm which is in the range of insulating materials. The conductivity at that lower temperature range is constant ($\sigma_c$) and characterizes the structure of the investigated glass samples. The increasing of measuring temperature up to 475 K enhances the dc-conductivity to about 3.5 decades higher for all investigated samples.

## References


[1.] K. Kirdsiri, J. Kaewkhao, A. Pokaipisit, W. Chewpraditkul, P. Limsuwan, Gamma-rays shielding properties of xPbO:(100–x)$B_2O_3$ glasses system at 662 keV. Ann. Nucl. Energy **36**, 1360–1365 (2009)

[2.] P. Yasaka, N. Pattnaboonmee, H.J. Kim, P. Limkitjaroenporn, J. Kaewkhao, Gamma radiation shielding and optical properties measurements of zinc bismuth borate glasses. Ann. Nucl. Energy **68**, 4–9 (2014)

[3.] C. Stehle, C. Vira, D. Hogan, S. Feller, M. Affatigato, Optical and physical properties of bismuth borate glasses related to structure. Phys. Chem. Glasses **39**, 83–86 (1998)

[4.] M. Sathish, B. Eraiah, Synthesis, characterization and optical properties of niobium doped silver-lead-borate glasses. Int. J. Eng. Res. Appl. **2**, 1264–1270 (2012)

[5.] Y.S. Rammah, M.I. Sayyed, A.S. Abohaswa, H.O. Tekin, FTIR, electronic polarizability and shielding parameters of $B_2O_3$ glasses doped with $SnO_2$. Appl. Phys. A **124**, 650 (2018)

[6.] A. Terczynska-Madej, K. Cholewa-Kowalska, M. Łączka, J. Opt. Mater. **33**, 12 (2011)

[7.] V. Martin, B. Wood, U. Werner-Zwanziger, J. Zwanziger, Structural aspects of the photoelastic response in lead borate glasses. J. Non-Cryst. Solids **357**, 2120 (2011)

[8.] Z. Pan, S. Morgan, B. Long, J. Non-Cryst. Solids **185**, 127 (1995)

[9.] T. Takaishi, J. Jin, T. Uchino, T. Yoko, J. Am. Ceram. Soc. **83**, 2543 (2000)

[10.] M.S. Dahiya, S. Khasa, A. Yadav, A. Agarwal, Appearance of small polaron hopping conduction in iron modified cobalt lithium bismuth borate glasses. AIP Conf. Proc. **1731**, 70018 (2016)

[11.] F.H. Margha, G.T. El-Bassyouni, G.M. Turky, Enhancing the electrical conductivity of vanadate glass system ($Fe_2O_3$, B2O3, V2O5) via doping with sodium or strontium cations. Ceram. Int. **45**, 11838–11843 (2019). https://doi.org/10.1016/j.ceramint.2019.03.064)

[12.] S. Khasa, A. Yadav, M.S. Dahiya, A. Agarwal, Effect of mixed transition metal ions on DC conductivity in lithium bismuth borate glasses. AIP Conf. Proc. **1665**, 070013 (2015)

[13.] G.M. Turky, M. Dawy, Spectral and electrical properties of ternary ($TeO_2$ – $V_2O_5$ – $Sm_2O_4$) glasses. Mater. Chem. Phys. **77**, 48 (2002)

[14.] A. Yadav, M.S. Dahiya, P. Narwal, A. Hooda, A. Agarwal, S. Khasa, Electrical characterization of lithium bismuth borate glasses containing cobalt/vanadium ions. Solid State Ionics **312**, 21–31 (2017)

[15.] R.M.M. Morsi, S. Ibrahim, S.A. Naf, M.M. Morsi, Effect of alkaline earth metal oxides on the dielectric, structural and physico-chemical properties of lithium-zinclead-borates. J. Mater. Sci. Mater. Electron. **27**, 4147–4156 (2016)

[16.] G. Paramesh, K.B.R. Varma, Near constant loss dielectric response in $2Bi_2O_3$–$B_2O_3$ glasses. Int. J. Appl. Glas. Sci. **2**, 235–242 (2011)

[17.] D.M. Laughman, R.D. Banhatti, K. Funke, Phys. Chem. Chem. Phys. **11**(17), 3158 (2009)

[18.] D.M. Laughman, R.D. Banhatti, K. Funke, Phys. Chem. Chem. Phys. **12**(42), 14102 (2010)

[19.] D.P. Singh, K. Shahi, K.K. Kar, Superlinear frequency dependence of AC conductivity and its scaling behavior in xAgI-(1–x) $AgPO_3$ glass superionic conductors. Solid State Ionics **287**, 89–96 (2016)

[20.] M. Cutroni, A. Mandanici, P. Mustarelli, C. Tomasi, Conductivity dynamical response in (AgI)x($AgPO_3$)1x glasses. Solid State Ionics **154–155**, 713–717 (2002)

[21.] N.S. El-Sayed, M.E. Abd El-Aziz, S. Kamel, G. Turky, Synthesis and characterization of polyaniline/tosylcellulose stearate composites as promising semiconducting materials. Synth. Met. **236**, 44–53 (2018)

[22.] M.E. Abd-El-Aziz, A.M. Youssef, S. Kamel, G. Turky, Conducting hydrogel based on chitosan, polypyrrole and magnetite nanoparticles: a broadband dielectric spectroscopy study. Polym. Bull. **76**, 3175–3194 (2019)

[23.] M. Moniruzzama, K.I. Winey, Polymer nanocomposites containing carbon nanotubes. Macromolecules **39**, 5194–5205 (2006)

[24.] M.A. Moussa, M.H. Abdel Rehim, S.A. Khairy, M.A. Soliman, A.M. Ghoneim, G.M. Turky, Electrical investigations of polyaniline/sulfonated polystyrene composites using broadband dielectric spectroscopy. Synth. Met. **209**, 34–40 (2015)

[25.] P. Dutta, S. Biswas, M. Ghosh, S. De, S. Chatterjee, The dc and ac conductivity of polyaniline– polyvinyl alcohol blends. Synth. Met. **122**, 455–461 (2001)

[26.] A.M. Milankovic, A. Santic, V. Licina, D.E. Day, Dielectric behavior and impedance spectroscopy of bismuth iron phosphate glasses. J. Non-Cryst. Solids **351**, 3235–3245 (2005)

[27.] A. Langar, N. Sdiri, H. Elhouichet, M. Ferid, Conductivity and dielectric behavior of $NaPO_3$–ZnO–$V_2O_5$ glasses. J. Alloys Compd. **590**, 380–387 (2014)

[28.] P.B. Macedo, C.T. Moynihan, R. Bose, Phys. Chem. Glasses **13**, 171 (1972)

[29.] N.S. El-Sayed, M.A. Moussa, S. Kamel, G. Turky, Development of electrical conducting nanocomposite based on carboxymethyl cellulose hydrogel/silver nanoparticles@polypyrrole. Synth. Met. **250**, 104–114 (2019)

[30.] Y.S. Rammah, A. Askin, A.S. Abouhaswa, F.I. El-Agawany, M.I. Sayyed, Synthesis, physical, structural and shielding properties of newly developed $B_2O_3$–ZnO–PbO–$Fe_2O_3$ glasses using Geant4 code and WinXCOM program. Appl. Phys. A **125**, 523 (2019)

[31.] M.A. Mohamed, S.M. Abo-Naf, H.A. Zayed, N.S. Hassan, Photoluminescence and semiconducting behavior of Fe Co Ni and Cu implanted in heavy metal oxide glasses. J. Mater. Res. Technol. **5**(3), 226–233 (2016)

[32.] G.R. Sundari, D.V. Sathish, T.R. Rao, C.R. Krishna, C.V. Reddy, R.V.S.S.N. Ravikumar, Characterization of $Fe^{3+}$ doped mixed alkali zinc borate glasses – physical and spectroscopic investigations. J. Non-Cryst. Solids **365**, 6–12 (2013)

[33.] D.A. Rayan, Y.H. Elbashar, M.M. Rashad, A. El-Korashy, Spectroscopic analysis of phosphate barium glass doped cupric oxide for bandpass absorption filter. J. Non Cryst. Solids **382**, 52–56 (2013)

[34.] J. Tauc, *Amorphous and Liquid Semiconductors*, ed. by J. Tauc (Plenum Press, New York, 1974).

[35.] N.F. Mott, E.A. Davies, *Electronic Processes in Non-Crystalline Materials* (Clarendon Press, Oxford, 1979)

[36.] F. Urbach, The long-wavelength edge of photographic sensitivity and of the electronic absorption of solids. Phys. Rev. **92**, 3124 (1953)

[37.] V. Raja, A.K. Sarma, V.N. Rao, Optical properties of pure and doped PMMA-CO-$P_4$VPNO polymer films. Mater. Lett. **57**(30), 4678–4683 (2003)

[38.] F. Yakuphanoglu, G. Barım, I. Erol, Phys. B **391**, 136 (2007)

[39.] Y.S. Rammah, A.A. Ali, R. El-Mallawany, A.M. Abdelghany, Optical properties of bismuth borotellurite glasses doped with $NdCl_3$. J. Mol. Struct. **1175**, 504–511 (2019)

[40.] S.H. Wemple, M. DiDomenico Jr., Behavior of the electronic dielectric constant in covalent and ionic materials. Phys. Rev. B **3**, 1338 (1971)

[41.] A.M. El Sayed, S. El-Sayed, W.M. Morsi, S. Mahrous, A. Hassen, Polym. Comp. **35**, 1842 (2014)

[42.] O.G. Abdullah, D.A. Tahir, K. Kadir, J Mater. Sci. Mater. Electron. **26**, 6939 (2015)

[43.] H. Vogel, The law of the relation between the viscosity of liquids and the temperature. Phys. Z. **22**, 645–646 (1921)

[44.] G.S. Fulcher, Analysis of recent measurements of the viscosity of glasses. J. Am. Ceram. Soc. **8**, 339–355 (1925)

[45.] G. Tammann, W. Hesse, Die Abhaengigkeit der Viskositat von der Temperatur bei unterkühlten Flüssigkeiten. Z. für Anorg. Allg. Chem. **156**, 245–257 (1926)

[46.] S. Dalal, S. Khasa, M.S. Dahiya, A. Agarwal, A. Yadav, V.P. Seth, S. Dahiya, Effect of substituting iron on structural, thermal and dielectric properties of lithium borate glasses. Mater. Res. Bull. **70**, 559–566 (2015)

[47.] ShSh Omara, G.M. Turky, A.M. Ghoneim, A.F. Thünemann, M.H. Abdel Rehim, A. Schönhals, Hyperbranched poly(amidoamine)/kaolinite nanocomposites: Structure and charge carrier dynamics. Polymer **121**, 64–74 (2017)

[48.] A.G. Darwish, G. Turky, M.Y. Hassaan, A. Ghoneim, Impact of RGO on electrical and dielectric properties of $Co_3O_4$/RGO nanocomposite. Mater. Res. Express **6**, 105039 (2019)